Quantum Hall drag of exciton condensate in graphene

Xiaomeng Liu[1], Kenji Watanabe[2], Takashi Taniguchi[2], Bertrand I. Halperin[1] and Philip Kim[1]*

An exciton condensate is a Bose–Einstein condensate of electron and hole pairs bound by the Coulomb interaction[1,2]. In an electronic double layer (EDL) subject to strong magnetic fields, filled Landau states in one layer bind with empty states of the other layer to form an exciton condensate[3–9]. Here we report exciton condensation in a bilayer graphene EDL separated by hexagonal boron nitride. Driving current in one graphene layer generates a near-quantized Hall voltage in the other layer, resulting in coherent exciton transport[4,6]. Owing to the strong Coulomb coupling across the atomically thin dielectric, quantum Hall drag in graphene appears at a temperature ten times higher than previously observed in a GaAs EDL. The wide-range tunability of densities and displacement fields enables exploration of a rich phase diagram of Bose–Einstein condensates across Landau levels with different filling factors and internal quantum degrees of freedom. The observed robust exciton condensation opens up opportunities to investigate various many-body exciton phases.

An exciton Bose–Einstein condensate (BEC) is formed when a large fraction of excitons occupy the ground state, establishing macroscopic coherence with weak dipolar repulsion[1,3]. However, optically generated excitons have short lifetimes. They can quickly recombine and release a photon, which leads to the annihilation of excitons. By trapping the released photon in an optical cavity, recent studies have shown the BEC of exciton-polaritons, consisting of a superposition of an exciton and a photon[10–13]. Another way to achieve a large density of long-lived excitons is to place electrons and holes in spatially separated parallel conducting layers, where excitons can form across the layers. In semiconducting EDLs, such indirect excitons can be formed by optical excitation[14] or electrical doping[15]. One salient feature of the exciton BEC is dissipationless exciton transport, consisting of counter-flowing electrical currents carried by co-travelling electrons and holes[4]. The first experimental observation of this superfluid exciton flow was demonstrated in GaAs EDLs under a strong magnetic field, in which a strong correlation is formed between electron-like and hole-like quasiparticles in quantizing orbits[3–9].

The magnetic-field-induced layer coherence of the EDL can be established in the following way. When a two-dimensional (2D) electron gas of density n is subject to a perpendicular magnetic field B, the kinetic energy of electrons is quantized to discrete Landau levels (LLs). Each LL contains $n_0 = (eB/h)$ degenerate Landau orbits per unit area, where e is electron charge and h is Planck's constant. If all the orbits in a LL are occupied (that is, the filling factor $\nu = n/n_0$ is an integer), the 2D electron system forms a quantum Hall state. In the EDL, the filling factor of the individual layer can be specified by $\nu_{\text{top}} = n_{\text{top}}/n_0$ and $\nu_{\text{bot}} = n_{\text{bot}}/n_0$, where n_{top} and n_{bot} are the density of top and bottom layer, respectively. If LLs in

both layers are partially filled—that is, ν_{top} and ν_{bot} are non-integer numbers—then neither layer can form a quantum Hall state on its own. However, Coulomb repulsion forces the electrons in the two layers to occupy different orbitals in space, leading to spatial anti-correlation between layers. Notably, when the total filling fraction, $\nu_{\text{tot}} = \nu_{\text{top}} + \nu_{\text{bot}}$, becomes an integer, the two layers together can form a coherent state in which each filled state (quasi-electron) in one layer corresponds to an empty state (quasi-hole) in the other layer. These bound empty–filled states can be described as excitons in the quantum Hall scenario and yield a strong response in the Coulomb drag experiment: driving current in one layer generates a quantized Hall drag voltage in the other layer. To be specific, the ratio between Hall drag voltage (V_{xy}^{drag}) and drive current (I^{drive}), defined as Hall drag resistance, is then quantized as $R_{xy}^{\text{drag}} = V_{xy}^{\text{drag}}/I^{\text{drive}} = h/\nu_{\text{tot}}e^2$. Meanwhile, Hall resistance of the drive layer (R_{xy}^{drive}), obtained from the drive Hall voltage (V_{xy}^{drive}), is also quantized to the same value despite having a partially filled LL, while the longitudinal voltages in both layers vanishes.

Quantized Hall drag for $\nu_{\text{tot}} = 1$ has been observed in the lowest LLs in GaAs EDLs[6]. Coherent tunnelling between the layers[5] and perfect current drag measurements[9] further confirmed the presence of the interlayer coherence and the superfluid exciton flow. The BEC realized in semiconducting EDLs, however, turns out to be rather fragile, with a BEC transition temperature T_c in the sub-kelvin range. This fragility is mainly caused by the relatively large EDL separation d required. It is noted that T_c is proportional to the characteristic energy scale $e^2/\varepsilon l$, where ε is the dielectric constant and $\ell = (\hbar/eB)^{1/2}$ is the magnetic length, specifying the distance between quasiparticles in a LL (refs 16,17). Also, the exciton BEC appears only in the strong-coupling regime[4], where the ratio d/ℓ is below the critical value of $d/\ell < 2$. Thus, reducing d substantially below the limit of the semiconducting EDL will likely enhance T_c and increase the exciton binding energy.

Recent progress on 2D van der Waals heterostructures has created a new opportunity to build EDLs using atomically thin materials[18–21]. Owing to electron–hole symmetry and extremely light carrier mass, EDLs consisting of mono- and bilayer graphene have been of particular interest to realize an exciton BEC (refs 22–25). Furthermore, tunnelling currents in graphene–hBN–graphene heterostructures are not appreciable when $d > 1.5$ nm at small biases, due to the large bandgap of hBN and the lattice direction mismatch between graphene layers[18,26]. Initial experiments performed in graphene–hBN–graphene heterostructures demonstrated a strong Coulomb drag effect in the semiclassical regime realized at high temperatures, exhibiting the strong interaction between the two layers in zero and finite magnetic fields[18–20]. However, experimental evidence of interlayer coherence has yet to be found. In this work, with improved device quality and fabrication techniques

[1]Department of Physics, Harvard University, Cambridge, Massachusetts 02138, USA. [2]National Institute for Material Science, 1-1 Namiki, Tsukuba 305-0044, Japan. *e-mail: pkim@physics.harvard.edu
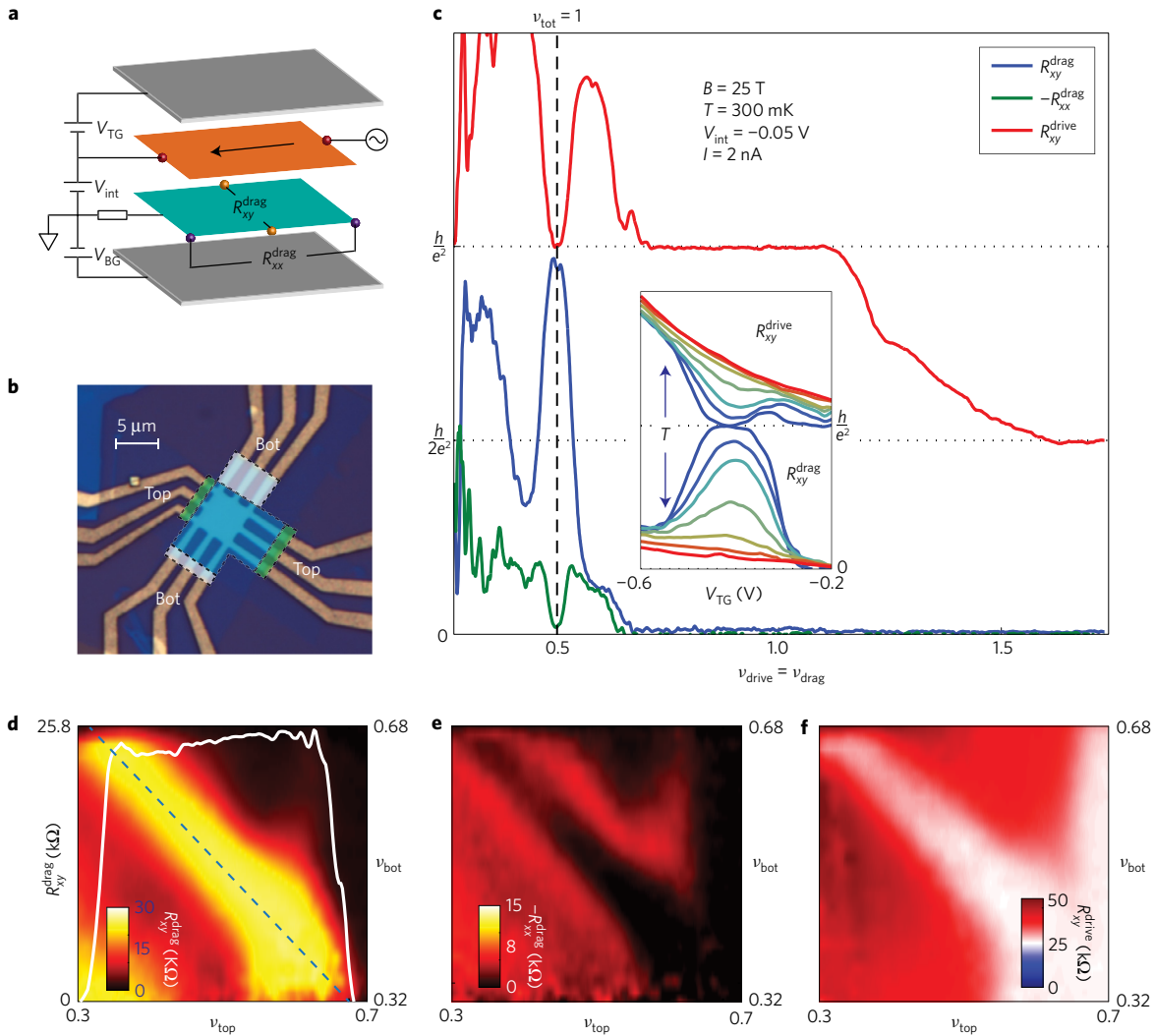
Figure 1 | Quantized Hall drag for $\nu_{tot} = 1$ state in bilayer graphene double layers. a, Schematic diagram of device and measurement set-up. **b**, Optical microscope image of the device. Metal leads on the left and right of the image (three on each side) contact the top layer graphene, while others contact the bottom layer graphene. The blue shaded area of graphene is under the top gate; white and green shaded regions are under the contact gate. The contact gates support highly transparent electrical contacts under high magnetic fields, providing reliable data away from the $\nu = 0$ insulating state. **c**, R_{xy}^{drag}, R_{xx}^{drag}, R_{xy}^{drive} as a function of filling factors of both layers at $B = 25$ T and $T = 300$ mK. The exciton BEC can be recognized by near-quantized Hall drag ($R_{xy}^{drag} = h/e^2$, $R_{xx}^{drag} = 0$) with the simultaneous re-entrant quantum Hall in the drive layer. (Inset) Temperature dependence ($T = 0.9$, 2.29, 3.13, 4.35, 6, 8, 10 K) of R_{xy}^{drag} at $B = 25$ T. **d**-**f**, R_{xy}^{drag}, $-R_{xx}^{drag}$, R_{xy}^{drive}, respectively, as a function of filling fractions ν_{top} and ν_{bot}, computed from V_{TG} and V_{BG}. The exciton BEC region appears as a diagonal region satisfying $\nu_{top} + \nu_{bot} = 1$. The white trace in **d** shows the value of R_{xy}^{drag} (axis on the left) along the $\nu_{tot} = 1$ line (dashed line in **d**). For further quantitative analysis, we also present several traces of the colour plot in Supplementary Fig. 11.

(see Supplementary Information), we demonstrate magnetic-field-induced exciton condensation in graphene EDL.

Our devices are made of two Bernal-stacked bilayer graphene sheets separated by 3 nm hBN and encapsulated by two thicker hBN layers (20–30 nm) (Fig. 1a,b). The two graphene layers are independently contacted by multiple electrodes (see Supplementary Information for details). Both graphene layers have mobility $0.5 \sim 1 \times 10^6$ cm^2 V^{-1} s^{-1} and exhibit symmetry-breaking quantum Hall states at fields as low as 5 T (Supplementary Figs 3 and 4). No appreciable tunnelling current is measured above the noise level, providing a lower bound on the tunnelling resistance of 1 GΩ. The voltages applied to the top gate (V_{TG}), the bottom gate (V_{BG}) and the interlayer bias between graphene layers (V_{int}) tune the carrier densities of the top and bottom graphene layers (n_{top}, n_{bot}): $n_{top} = C_{TG} V_{TG} - C_{int} V_{int}$; $n_{bot} = C_{BG} V_{BG} + C_{int} V_{int}$. Here C_{TG}, C_{BG}, and C_{int}, are capacitances between the top gate and top layer, the bottom gate and bottom layer, and between the top and bottom graphene layers, respectively. By controlling V_{TG}, V_{BG}, and V_{int}, we can also

adjust the average displacement fields; $D_{top} = (C_{TG} V_{TG} + C_{int} V_{int})/2$ and $D_{bot} = (-C_{BG} V_{BG} + C_{int} V_{int})/2$, for the top and bottom layers, respectively. For the drag measurements, we apply current I^{drive} only in the top layer and measure the Hall resistance (R_{xy}^{drive}) of the current-carrying (drive) layer and magneto- and Hall drag resistances (R_{xx}^{drag} and R_{xy}^{drag}) of the drag layer under a perpendicular magnetic field B. Owing to the Onsager relation, switching the drive and drag layer produces experimentally equivalent drag results (Supplementary Fig. 5).

Figure 1c shows measurements of R_{xy}^{drive}, $-R_{xx}^{drag}$ and R_{xy}^{drag} under $B = 25$ T, corresponding to the strong-coupling limit ($l = 5.1$ nm and $d/l = 0.58$). In this plot, we adjust V_{TG} and V_{BG} such that the filling fractions of each layer are balanced ($\nu \equiv \nu_{drive} = \nu_{drag}$). We observe that each layer exhibits its own quantum Hall effect (QHE). For $\nu \geq 1$, R_{xy}^{drive} exhibit QH plateaus at the values $(R_{xy}^{drive})^{-1} = (e^2/h)$, $(4/3)(e^2/h)$, $(2e^2/h)$. In these well-developed integer ($\nu = 1, 2$) and fractional ($\nu = 4/3$) QH regimes of the individual layers, we find no appreciable drag signal
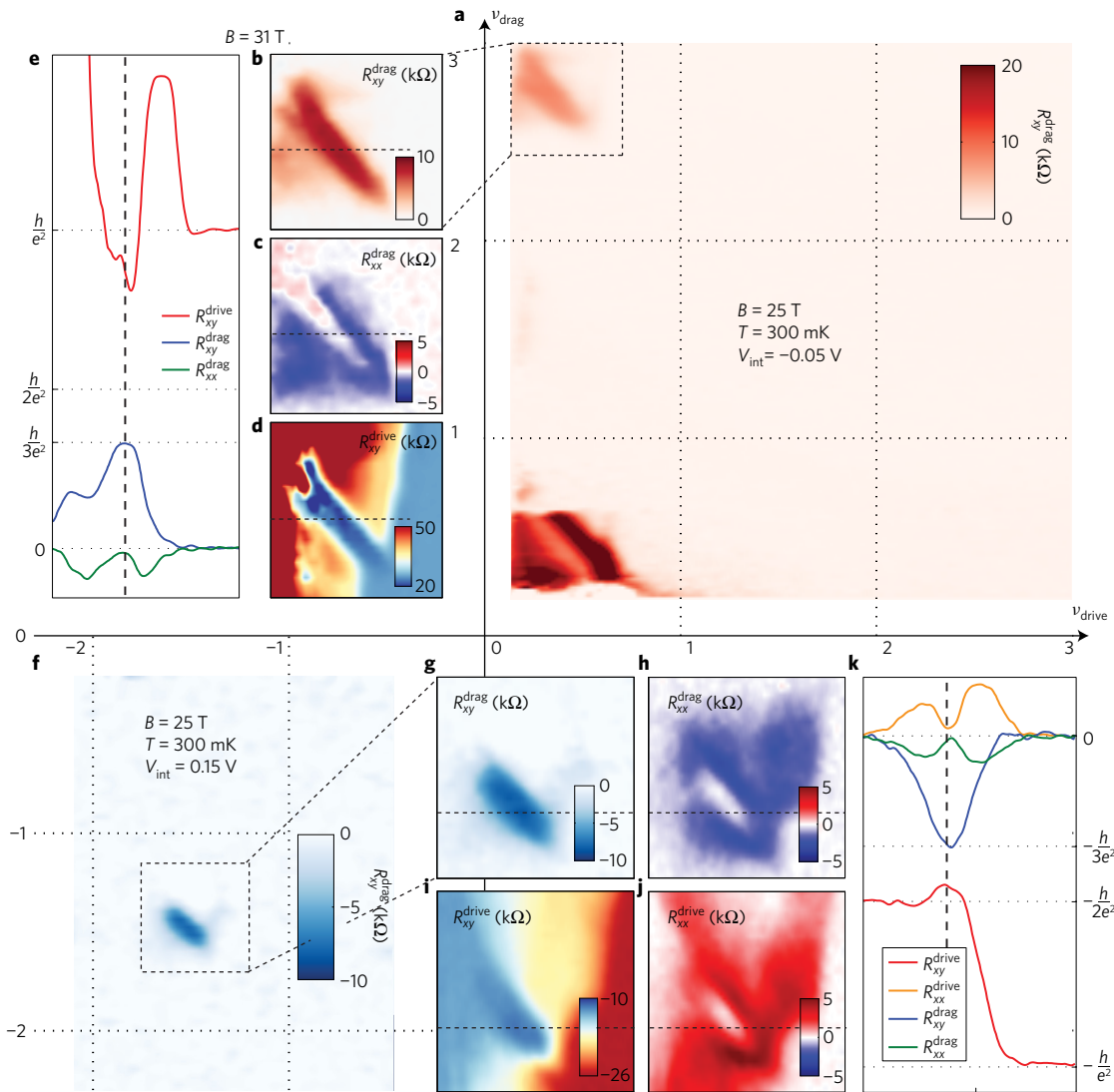
Figure 2 | Exciton BEC in various LL fillings. a, R_{xy}^{drag} as a function of the top and bottom layer filling factors at $B=25$ T, $T=300$ mK and $V_{int}=-0.05$ V. Besides $(\nu_{drag}, \nu_{drive})=(0.5, 0.5)$, a different exciton BEC state is found near $(0.5, 2.5)$. **b–d**, Zoomed-in plot of $R_{xy}^{drag}, R_{xx}^{drag}, R_{xy}^{drive}$, respectively, around $\nu_{tot}=3$ at a higher field of $B=31$ T. **e**, Line-cuts of $R_{xy}^{drag}, R_{xx}^{drag}, R_{xy}^{drive}$ along the dashed lines shown in **b–d**, respectively. **f**, R_{xy}^{drag} as function of filling factors at $B=25$ T, $T=300$ mK and $V_{int}=0.15$ V. Additional exciton BEC state in the hole–hole regime is identified around $(\nu_{drag}, \nu_{drive})=(-1.5, -1.5)$. **g–j**, $R_{xy}^{drag}, R_{xx}^{drag}, R_{xy}^{drive}, R_{xx}^{drive}$, respectively, at the same condition as **f**. **k**, Line-cuts of $R_{xy}^{drag}, R_{xx}^{drag}, R_{xy}^{drive}, R_{xx}^{drive}$ along the dashed lines shown in **g–j**, respectively. The horizontal dashed lines in **e** and **k** indicate $\pm(h/3e^2)$, to which R_{xy}^{drag} and R_{xy}^{drive} are expected to be quantized.

$(R_{xx}^{drag} \approx R_{xy}^{drag} \approx 0)$. The vanishing drag signals at low temperatures are expected in the semiclassical picture due to the diminishing scattering phase space[27]. However, the observed drag signals are significantly enhanced when the first LL of both layers are partially filled $(\nu < 1)$. In particular, for $\nu = 1/2$, where both layers are half-filled and thus $\nu_{tot} = \nu_{drive} + \nu_{drag} = 1$, the Hall drag signal reaches close to the quantization value of $h/e^2 = 25.8$ kΩ, while the magneto-drag (R_{xx}^{drag}) dips to nearly zero. Under the same condition, the Hall resistance in the drive (top) layer, which originally rises beyond h/e^2 as ν_{drive} drops below one (corresponding to partially filled LL), re-enters h/e^2 again at $\nu_{tot} = 1$. This re-entrant behaviour of R_{xy}^{drive} to the same quantized value of R_{xy}^{drag} indicates that the entire EDL behaves like a single $\nu = 1$ quantum Hall system despite that LLs in each layer are only partially filled.

The quantized Hall drag and re-entrant QHE in the drive layer have been observed previously in GaAs EDLs for $\nu_{tot} = 1$ and are considered as a strong evidence of interlayer coherence and exciton superfluidity[6]. We note, however, the unambiguous demonstration of superfluidity and coherence requires further measurements. A simple physical picture for the observed quantized Hall drag can be built upon a two-fluid picture. In this model, currents in each layer are carried by excitons in the bulk $(I_{ex}^{(i)})$ and quasiparticles flowing on the edge $(I_{qp}^{(i)})$, where the superscript is the layer index. Excitons generate counter-flow currents $I_{ex}^{drag} = -I_{ex}^{drive}$; and the zero accelerating electric force requirement on superfluid excitons demands $V_{xy}^{drive} = V_{xy}^{drag} = V_{xy}$. In addition, boundary conditions of the drag and drive layers requires $I_{ex}^{drag} + I_{qp}^{drag} = 0$, $I = I_{ex}^{drive} + I_{qp}^{drive}$. Furthermore, by considering the two layers as a single coherent quantum Hall system at filling fraction ν_{tot}, we have $I_{qp} = I_{qp}^{drag} + I_{qp}^{drive} = (\nu_{tot}e^2/h)V_{xy}$. Summing up, we obtain the experimental observation $R_{xy}^{drive} = R_{xy}^{drag} = h/\nu_{tot}e^2$ with vanishing R_{xx}^{drag} and R_{xx}^{drive}.

We found that the observed quantized Hall drag in graphene is much more robust than that of the GaAs EDLs. The signatures of the exciton condensate—nearly quantized R_{xy}^{drag} and re-entry behaviour of R_{xy}^{drive}—persist up to a few kelvin for $\nu_{tot} = 1$ at $B = 25$ T (Fig. 1c inset). For quantitative analysis, we compute the counter-flow resistances $(R_{xy}^{CF}$ and $R_{xx}^{CF})$ and plot them as a function of $1/T$ at $\nu_{tot} = 1$ (Supplementary Fig. 7). Although the theoretical expectation

for 2D BEC transition is the Kosterlitz–Thouless transition[16,28], we find that the vanishing R_{xy}^{CF} and R_{xx}^{CF} exhibit thermally activating behaviour similar to what has been observed in the GaAs system[6]. However, the activation gap we obtained ($\Delta \approx 8\,\mathrm{K}$) is ten times larger than previous reported (Supplementary Fig. 7b).

The exciton BEC in graphene is also found to be robust against the density imbalance between layers[29]. The signatures of the exciton condensation—that is, $R_{xy}^{drag} \approx R_{xy}^{drive} \approx h/e^2$ and $R_{xx}^{drag} \approx R_{xx}^{drive} \approx 0$—withstand a range of gate voltages satisfying $\nu_{drag} + \nu_{drive} = 1$, corresponding to the diagonal line specified in Fig. 1d–f. For a more quantitative analysis, we plot the R_{xy}^{drag} cut along this diagonal line as an overlay graph in Fig. 1d (white trace). The level of R_{xy}^{drag} quantization indicates that the BEC persists for the density imbalance ($\Delta n/n_{tot}$) = $(n_{drag} - n_{drive})/(n_{drag} + n_{drive})$ up to $\sim\pm30\%$. Beyond this limit the more stable integer QH states (ν_{drag} or $\nu_{drive} = 0$ or 1) in each layer take over the exciton BEC phase.

Although the exciton BEC has been discovered only for the half-filled lowest LL in the GaAs EDLs, the gate tunability in graphene EDL devices allows us to explore the phase diagram of possible condensate states other than $\nu_{tot} = 1$. Figure 2 shows an experimental survey for R_{xy}^{drag} as a function of ν_{drive} and ν_{drag}, covering the electron–electron ($\nu_{drive}, \nu_{drag} > 0$) and hole–hole ($\nu_{drive}, \nu_{drag} < 0$) regimes. Remarkably, we find at least two additional interlayer correlated states in these regimes: (ν_{drive}, ν_{drag}) centred near (0.35, 2.65) and (−1.5, −1.5), corresponding to the drag between $(1/2) - 2(1/2)$ filled electron LLs ($\nu_{tot} = 3$) and $1(1/2) - 1(1/2)$ filled hole LLs ($\nu_{tot} = -3$), respectively. Similar to the BEC in $\nu_{tot} = 1$, these states exhibit the near-quantized Hall drag $R_{xy}^{drag} \approx h/\nu_{tot}e^2$ and $R_{xx}^{drag} \approx 0$, for a range of (ν_{drive}, ν_{drag}) satisfying $\nu_{drive} + \nu_{drag} = \nu_{tot}$ (see Fig. 2b–j). These Hall drag features appear as diagonals in the (ν_{drive}, ν_{drag}) plots, and are confined to the sectors corresponding to partially filled first (drive) and third (drag) electron LLs (with all symmetries are lifted) and partially filled second (drive and drag) hole LLs. Although we cannot rule out other possible scenarios compatible with the experimental observations, we interpret these interlayer correlated states as exciton BEC for $\nu_{tot} = \pm3$. Measurements at lower magnetic fields also reveal a signature of a developing exciton BEC for (ν_{drive}, ν_{drag}) = (2.5, 0.5), the symmetric pair for (0.5, 2.5) discussed above (Supplementary Figs 5 and 8). The relatively weak presence of this symmetric pair is presumably due to the quality difference between the top and bottom graphene layers. We also remark that while $R_{xy}^{drag} \approx h/\nu_{tot}e^2$ and $R_{xx}^{drag} \approx R_{xx}^{drive} \approx 0$ are observed in the $\nu_{tot} = \pm3$ state, we find $|R_{xy}^{drive}| > h/\nu_{tot}e^2$ (Fig. 2e,k). Together with less developed quantization of R_{xy}^{drag} in these states, compared to $\nu_{tot} = 1$, we speculate that a dissipative exciton transport of a fragile BEC is responsible for this incomplete re-entrant QHE.

Interestingly, our experimental observations strongly indicate that the apparent electron–hole symmetry of LLs is broken for the exciton BEC. For example, the (0.5, 0.5) BEC exists while (−0.5, −0.5) is absent. The electron–hole asymmetry has been observed in the filling fraction sequences of the fractional quantum Hall effect in bilayer graphene and related with the orbital degeneracy of bilayer graphene LLs (ref. 30).

We note that the existence of the exciton BEC at fixed (ν_{drive}, ν_{drag}) depends sensitively on V_{int} (Fig. 3 and Supplementary Figs 8–10). When the density of each layer is kept close to half-filling by coordinately tuning V_{BG} and V_{TG}, V_{int} changes the displacement field exerted on both layers, $D_{top} = C_{int}V_{int} + n_{top}/2$ and $D_{bot} = C_{int}V_{int} - n_{bot}/2$. Figure 3c shows R_{xy}^{drag} as a function of D_{top} (top axis of Fig. 3b) and D_{bot} (bottom axis of Fig. 3d) while keeping $\nu_{tot} = 1$ at $B = 13\,\mathrm{T}$, $T = 1.5\,\mathrm{K}$. We observe that R_{xy}^{drag} undergoes multiple distinct transitions between high and low values as V_{int} changes. By comparing the displacement fields of these transitions with those of the integer quantum Hall transitions of each layer (Fig. 3b,d and Supplementary Fig. 10a), we found a close connection between the Hall drag and the LL character of each layer.
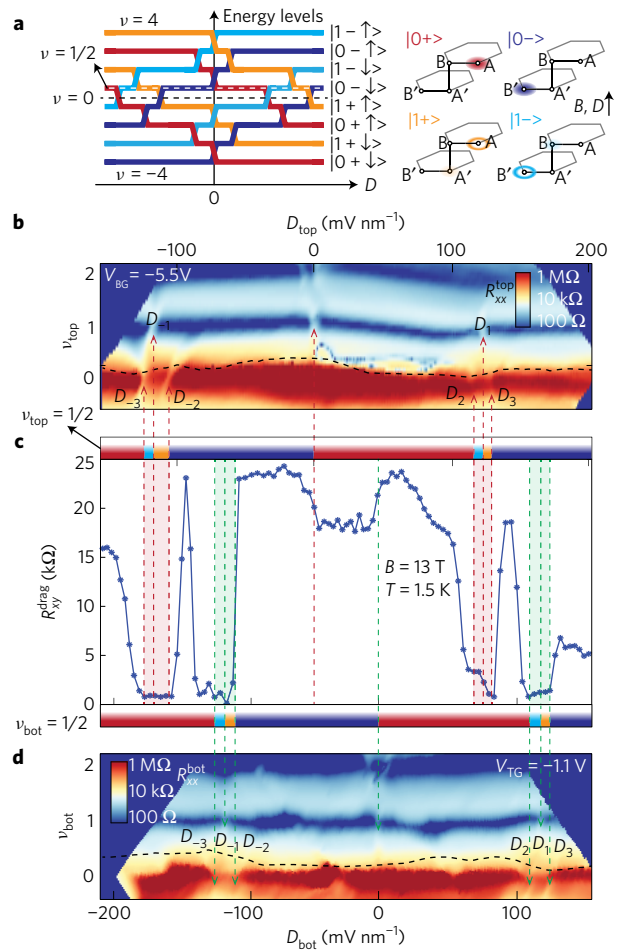

Figure 3 | Phase transition of $\nu_{tot} = 1$ exciton BEC induced by transverse electric field. a, Schematic diagram of Landau levels sequence (left) and wavefunctions (right) of bilayer graphene QHFM states for the lowest LL corresponding to $-4 < \nu < 4$. In the left diagram, the x direction represents the displacement field D and coloured lines denote QHFM Landau levels with different orbital (0/1), layer ($+/-$) and spin ($\uparrow/\downarrow$) quantum numbers, as noted next to the lines. Different colours are used for different orbital and layer quantum numbers. As the displacement field changes, the coloured lines cross each other, representing QHFM transitions induced by the displacement field. The horizontal black dashed line marks charge neutrality ($\nu = 0$) and the horizontal white dashed line marks the Fermi level of the half-filled first LL ($\nu = 1/2$). The diagram on the right depicts wavefunctions of different bilayer graphene QHFM states, with the same colour code as the lines in the left diagram. **b** (**d**), Longitudinal resistance of top (bottom) bilayer graphene as a function of displacement D_{top} (D_{bot}) and density n_{top} (n_{bot}) at $B = 13\,\mathrm{T}$ and $T = 1.5\,\mathrm{K}$. The QHFM transitions are marked with arrows. The data in **b** is taken at a fixed $V_{BG} = -5.5\,\mathrm{V}$ and the data in **d** is taken at $V_{TG} = -1.1\,\mathrm{V}$. **c**, R_{xy}^{drag} (blue curve) as a function of D_{top} (top axis of **b**) or D_{bot} (bottom axis of **d**) for $\nu_{tot} = 1$ state at $B = 13\,\mathrm{T}$ and $T = 1.5\,\mathrm{K}$. Each data point is taken at a different V_{int}, with V_{BG} and V_{TG} tuned around $\nu_{tot} = 1$ to maximize R_{xy}^{drag} (filling factor ν_{top}, ν_{bot} calculated from the gate voltages are marked by the horizontal dashed line in **b** and **d**). The coloured bars on the top and bottom of the plot represent orbital and layer character of the half-filled LL ($\nu = 1/2$) of the top and bottom bilayer graphene with the same colour code as **a**. The orange and green shaded regions of the main plot which signify $N = 1$ orbital states of the top and bottom layer coincide well with where the Hall drag vanishes, indicating the $N = 1$ orbit is incapable of forming the exciton BEC phase.

For a single bilayer graphene, the lowest Landau level (LLL) have eight-fold degeneracy in the single particle picture (between $\nu = -4$ and $\nu = 4$). This SU(8) symmetry space consists of spin degeneracy

$|\uparrow\rangle$ and $|\downarrow\rangle$, valley degeneracy K and K' and orbital degeneracy of $N = 0, 1$ (refs 31–34). In high-quality samples, these symmetries are broken by quantum Hall ferromagnetism (QHFM), and different symmetry-breaking states can be found at different displacement fields for each filling factor[31–34]. The symmetry-breaking state $\nu = 1$ has three transition points at $D = 0$ and $D = \pm D_1$, and $\nu = 0$ has four transition points at $D = \pm D_2, \pm D_3$, which can be identified in Fig. 3b,d. Across these transitions, the fully filled LLs have different spin, valley or orbital indexes. For partially filled LLs, layer polarization and orbital character were identified by a recent study using capacitance measurements[34]. The partially filled LL $0 < \nu < 1$ is found to hold different layer- and orbital-polarized states at different displacement fields (Fig. 3a) (+/− denote the layer polarization, which is equivalent to valley polarization K/K' in the lowest LL, and 0/1 denote the orbital index). The transitions between these states line up with the transitions of $\nu = 1$ and $\nu = 0$ states with regard to the displacement field. In our experiment, the $\nu_{tot} = 1$ state is formed between two partially filled bilayer graphene with $0 < \nu_{top}, \nu_{bot} < 1$. We found that Hall drag is suppressed when the partially filled LLs of one bilayer graphene or both bilayer graphene are in the $N = 1$ orbital state (shaded regions in Fig. 3c and Supplementary Fig. 10). This also explains the absence of other integer total filling factor states and the broken electron–hole symmetry, as the $-1 < \nu < 0$ $(0 < \nu < 1)$ LL is polarized in the $N = 1$ $(N = 0)$ orbital state under the same displacement field; the latter is capable of forming an exciton BEC, whereas the former is not. We speculate that the inability of the $N = 1$ orbit to establish an interlayer correlated state is due to its broader spatial wavefunction (Fig. 3a right), and thus weaker interaction. Similarly, the weaker Hall drag signal in the region where $D_{top} > 0$ and $D_{bot} < 0$ can be related to the weaker interaction when the wavefunctions of the two bilayer graphene are further apart due to the opposite layer polarization.

Methods

Methods, including statements of data availability and any associated accession codes and references, are available in the online version of this paper.

References

1. Littlewood, P. B. *et al*. Models of coherent exciton condensation. *J. Phys. Condens. Matter* **16**, S3597–S3620 (2004).
2. Snoke, D. *et al*. Spontaneous Bose coherence of excitons and polaritons. *Science* **298**, 1368–1372 (2002).
3. Eisenstein, J. & MacDonald, A. Bose–Einstein condensation of excitons in bilayer electron systems. *Nature* 691–694 (2004).
4. Eisenstein, J. P. Exciton condensation in bilayer quantum Hall systems. *Annu. Rev. Condens. Matter Phys.* **5**, 159–181 (2014).
5. Spielman, I. B., Eisenstein, J. P., Pfeiffer, L. N. & West, K. W. Resonantly enhanced tunneling in a double layer quantum Hall ferromagnet. *Phys. Rev. Lett.* **84**, 5808–5811 (2000).
6. Kellogg, M., Spielman, I. B., Eisenstein, J. P., Pfeiffer, L. N. & West, K. W. Observation of quantized Hall drag in a strongly correlated bilayer electron system. *Phys. Rev. Lett.* **88**, 126804 (2002).
7. Kellogg, M., Eisenstein, J. P., Pfeiffer, L. N. & West, K. W. Vanishing Hall resistance at high magnetic field in a double-layer two-dimensional electron system. *Phys. Rev. Lett.* **93**, 36801 (2004).
8. Tutuc, E., Shayegan, M. & Huse, D. A. Counterflow measurements in strongly correlated GaAs hole bilayers: evidence for electron–hole pairing. *Phys. Rev. Lett.* **93**, 36802 (2004).
9. Nandi, D., Finck, A. D. K., Eisenstein, J. P., Pfeiffer, L. N. & West, K. W. Exciton condensation and perfect Coulomb drag. *Nature* **488**, 481–484 (2012).
10. Kasprzak, J. *et al*. Bose–Einstein condensation of exciton polaritons. *Nature* **443**, 409–414 (2006).
11. Byrnes, T., Kim, N. Y. & Yamamoto, Y. Exciton–polariton condensates. *Nat. Phys.* **10**, 803–813 (2014).
12. Deng, H., Weihs, G., Santori, C., Bloch, J. & Yamamoto, Y. Condensation of semiconductor microcavity exciton polaritons. *Science* **298** (2002).
13. Balili, R., Hartwell, V., Snoke, D., Pfeiffer, L. & West, K. Bose–Einstein condensation of microcavity polaritons in a trap. *Science* **316** (2007).
14. High, A. A. *et al*. Spontaneous coherence in a cold exciton gas. *Nature* **483**, 584–588 (2012).
15. Seamons, J. A., Morath, C. P., Reno, J. L. & Lilly, M. P. Coulomb drag in the exciton regime in electron–hole bilayers. *Phys. Rev. Lett.* **102**, 26804 (2009).
16. Yang, K. *et al*. Quantum ferromagnetism and phase transitions in double-layer quantum Hall systems. *Phys. Rev. Lett.* **72**, 732–735 (1994).
17. Moon, K. *et al*. Spontaneous interlayer coherence in double-layer quantum Hall systems: charged vortices and Kosterlitz–Thouless phase transitions. *Phys. Rev. B* **51**, 5138–5170 (1995).
18. Gorbachev, R. V. *et al*. Strong Coulomb drag and broken symmetry in double-layer graphene. *Nat. Phys.* **8**, 896–901 (2012).
19. Liu, X. *et al*. Coulomb drag in graphene quantum Hall double-layers. Preprint at http://arxiv.org/abs/1612.08308 (2016).
20. Li, J. I. A. *et al*. Negative Coulomb drag in double bilayer graphene. *Phys. Rev. Lett.* **117**, 46802 (2016).
21. Lee, K. *et al*. Giant frictional drag in double bilayer graphene heterostructures. *Phys. Rev. Lett.* **117**, 46803 (2016).
22. Min, H., Bistritzer, R., Su, J.-J. & MacDonald, A. Room-temperature superfluidity in graphene bilayers. *Phys. Rev. B* **78**, 121401 (2008).
23. Kharitonov, M. & Efetov, K. Electron screening and excitonic condensation in double-layer graphene systems. *Phys. Rev. B* **78**, 241401 (2008).
24. Perali, A., Neilson, D. & Hamilton, A. R. High-temperature superfluidity in double-bilayer graphene. *Phys. Rev. Lett.* **110**, 146803 (2013).
25. Skinner, B. Interlayer excitons with tunable dispersion relation. *Phys. Rev. B* **93**, 2 (2016).
26. Lee, G. H. Electron tunneling through atomically flat and ultrathin hexagonal boron nitride. *Appl. Phys. Lett.* **99**, 243114 (2011).
27. Narozhny, B. N. & Levchenko, A. Coulomb drag. *Rev. Mod. Phys.* **88**, 25003 (2016).
28. Wen, X.-G. & Zee, A. Neutral superfluid modes and 'magnetic' monopoles in multilayered quantum Hall systems. *Phys. Rev. Lett.* **69**, 1811–1814 (1992).
29. Champagne, A. R., Finck, A. D. K., Eisenstein, J. P., Pfeiffer, L. N. & West, K. W. Charge imbalance and bilayer two-dimensional electron systems at $\nu T = 1$. *Phys. Rev. B* **78**, 205310 (2008).
30. Kou, A. *et al*. Electron–hole asymmetric integer and fractional quantum Hall effect in bilayer graphene. *Science* **345**, 55–57 (2014).
31. Lambert, J. & Côté, R. Quantum Hall ferromagnetic phases in the Landau level $N = 0$ of a graphene bilayer. *Phys. Rev. B* **87**, 115415 (2013).
32. Maher, P. *et al*. Bilayer graphene. Tunable fractional quantum Hall phases in bilayer graphene. *Science* **345**, 61–64 (2014).
33. Lee, K. *et al*. Chemical potential and quantum Hall ferromagnetism in bilayer graphene. *Science* **345**, 58–61 (2014).
34. Hunt, B. M. *et al*. Competing valley, spin, and orbital symmetry breaking in bilayer graphene. Preprint at http://arxiv.org/abs/1607.06461 (2016).

Author contributions

X.L. performed the experiments and analysed the data. X.L. and P.K. conceived the experiment. X.L., B.I.H. and P.K. wrote the paper. K.W. and T.T. provided hBN crystals.

Competing financial interests

The authors declare no competing financial interests.

Methods

Sample fabrication. The five single-crystal layers of graphene and hBN (Supplementary Fig. 1a) are prepared by mechanical exfoliation and van der Waals (vdW) transfer technique[35]. During the process, we choose two strip-shape bilayer graphene and align them into a cross, so we can use the overlapped part as the main channel area while fabricating individual contacts onto the non-overlapped parts (Supplementary Fig. 1b). The edge contacts and the top gate are fabricated after etching the entire stack into the final device geometry. Usually, the parts of graphene near metal contacts are slightly doped and form unwanted PN junctions due to the mismatch in the metal-graphene work function. These contact-induced local PN junctions cause contact barriers under high magnetic fields. To address this problem, we fabricate local top gates (contact gates) to dope the area of graphene around the contacts. These contact gates are adjusted to highly dope graphene leads next to the metal electrodes with the same carrier type of the channel (Supplementary Fig. 1c).

Drag measurements. In most of our measurements, we use the top layer as the drive layer and the bottom layer as the drag layer (switching the drive and drag layers does not affect our drag experiment results as shown in Supplementary Fig. 5). We apply $I^{\mathrm{drive}} = 2$ nA a.c. current (17.7 Hz) to the drive layer and measure the voltage drop along the longitudinal direction in the drag layer to obtain V_{xx}^{drag}. We also measure the voltage drops along the perpendicular direction in the drag and drive layers to obtain V_{xy}^{drag} and V_{xy}^{drive}, respectively. The magneto and Hall drag resistances are obtained by $R_{xx}^{\mathrm{drag}} = V_{xx}^{\mathrm{drag}}/I^{\mathrm{drive}}$ and $R_{xy}^{\mathrm{drag}} = V_{xy}^{\mathrm{drag}}/I^{\mathrm{drive}}$ from this measurement. One of the contacts in the drag layer is connected to ground through a 1 MΩ resistor to allow the gates to tune the density of the drag layer.

A typical way to drive current in lock-in measurements is by applying an a.c. bias voltage V^{drive} on one side of the graphene channel while grounding the other side. However, in Coulomb drag measurements, biasing the drive layer employing this scheme can create spurious drag signals in the drag layer due to drive-bias-induced a.c. gating. Because of the finite contact and channel resistances of the drive layer, the direct biasing scheme raises the potential in the middle of the drive layer to $\sim V^{\mathrm{drive}}/2$ with respect to ground. Since the drag layer is grounded, an a.c. interlayer bias of $\sim V^{\mathrm{drive}}/2$ is produced accordingly. In the previous drag experiments performed in GaAs double quantum wells, it has been shown that this a.c. interlayer bias induces spurious drag signals[36]. To prevent the a.c. interlayer bias, we employ a bridge set-up[37] as shown in Supplementary Fig. 2. In this scheme, the initial 4 V a.c. voltage is reduced down to 4 mV through a voltage divider. Then this 4 mV a.c. voltage is fed into the bridge through a 1:1 ground-isolating transformer. By tuning the variable resistor in the bridge, we can adjust the a.c. electrical potential in the middle of the drive layer to approximate zero. The 4 mV is then converted into ~ 2 nA by passing through two 1 MΩ resistors in series. This set-up also allows us to control the d.c. interlayer bias V_{int}. To monitor the drive current, we measure the voltage across one of the two 1 MΩ resistors.

Data availability. The data that support the plots within this paper and other findings of this study are available from the corresponding author upon reasonable request.

References

35. Wang, L. *et al*. One-dimensional electrical contact to a two-dimensional material. *Science* **342,** 614–617 (2013).
36. Hill, N. P. R. *et al*. Frictional drag between parallel two-dimensional electron gases in a perpendicular magnetic field. *J. Phys. Condens. Matter* **8,** L557–L562 (1996).
37. Kellogg, M. *Evidence for Excitonic Superfluidity in a Bilayer Two-Dimensional Electron System* thesis (2005).